Open Ceramics 15 (2023) 100413

Contents lists available at ScienceDirect

Open Ceramics

journal homepage: www.sciencedirect.com/journal/open-ceramics

Assessment of in-vitro bioactivity, biodegradability and antibacterial activity of polymer-derived 3D printed åkermanite scaffolds

Fulden Dogrul [a,b,c], Vera Bednarzig [c], Hamada Elsayed [b,d], Liliana Liverani [c,e], Dušan Galusek [a,f], Enrico Bernardo [b,*], Aldo R. Boccaccini [c,**]

[a] FunGlass – Centre for Functional and Surface Functionalized Glass, Alexander Dubček University of Trenčín, Trenčín, Slovakia
[b] Department of Industrial Engineering, Università Degli Studi di Padova, Padova, Italy
[c] Institute of Biomaterials, Friedrich-Alexander-Universität Erlangen-Nürnberg (FAU), Cauerstraße 6, 91058 Erlangen, Germany
[d] Department of Glass Research, National Research Centre, Egypt
[e] DGS S.p.A., Rome, Italy
[f] Joint Glass Centre of the IIC SAS, TnU AD and FChFT STU, Centre for Functional and Surface Functionalized Glass, TnUAD, Trenčín, Slovakia

ARTICLE INFO

Keywords:
Åkermanite
Scaffold
Polymer-derived-ceramic
Direct ink writing (DIW)
Bioceramic
Bioactivity
Antibacterial activity
Cytocompatibility

ABSTRACT

Reticulated åkermanite ($Ca_2MgSi_2O_7$) 3D scaffolds were fabricated by direct ink writing of pastes based on a commercial silicone resin and fillers, such as calcium carbonate ($CaCO_3$) and magnesium hydroxide ($Mg(OH)_2$) microparticles, followed by heat treatment at 1100 °C in air. To form liquid phase upon firing and thus promote the ionic interdiffusion, borax ($Na_2B_4O_7{\cdot}10H_2O$) or hydrated sodium phosphate ($Na_2HPO_4{\cdot}12H_2O$) were considered as alternative additives. Although leading to scaffolds with different strength-to-density ratio, the two additives did not lead to substantial differences in terms of biological response. All fabricated ceramics exhibited acellular *in-vitro* bioactivity upon immersion in simulated-body-fluid (SBF) as well as antibacterial activity against *S. aureus* and *E. coli*. Direct contact cell viability test, performed with a stromal-cell line from mouse bone marrow (ST-2 cells), indicated no cytotoxicity of both samples determined by the WST-8 assay.

1. Introduction

Among bioceramics, those based on the CaO–MgO–SiO_2 system (bredigite $Ca_7MgSi_4O_{16}$, åkermanite $Ca_2MgSi_2O_7$ and diopside $CaMgSi_2O_6$) are attracting an increasing interest in the scientific community [1]. In particular, åkermanite is highly attractive due to its superior performance in terms of mechanical properties, controlled degradation rate and remarkable osteogenic features over calcium phosphates ($Ca_3(PO_4)_2$) and calcium silicate ($CaSiO_3$) [2,3]. According to *in-vitro* and *in-vivo* tests, it has been shown that the presence of Mg improves the strength and reduces the degradation rate significantly [4]. Concerning the antibacterial properties of silicate bio-ceramics, magnesium ions are not known to play a role. However, many studies showed an antibacterial effect of åkermanite ceramics related to the progressive increase of the solution pH and formation of an environment not suitable for bacterial growth [5]. Several evidences support, in addition, the fact that åkermanite bioceramics induce angiogenesis [1,6].

Preceramic polymers, particularly in the form of polysiloxanes (known also as 'silicones'), as feedstock for bioceramics [7–9] have been proposed as precursors for Ca-based silicate bioceramics [10]. After embedding micro- and nano-sized fillers, comprising carbonates, hydroxides or oxides, silicones (non-toxic and cost-effective) may be converted into the desired silicate phase, generally with excellent phase purity and at a relatively low temperature (900–1100 °C) [10]. A first key feature is the reactivity of the (abundant) amorphous silica residue of silicones fired in air. The stoichiometry of a 'target' silicate is easily achieved by proper control of the relative amounts of the silicone (the amount of silica may vary depending on the specific polymer [10]) and fillers. A second key feature, common to most preceramic polymers [11], is the possibility to apply various shaping technologies to fabricate components in the polymeric state, before heat treatment and ceramic conversion. Bioceramics can be prepared via polymer shaping methods, like direct foaming [10,12], as well as by additive manufacturing, including direct ink writing [10,13–15] and digital light processing [16].

Despite the high reactivity of the amorphous silica mentioned above,

* Corresponding author.
** Corresponding author.
E-mail addresses: enrico.bernardo@unipd.it (E. Bernardo), aldo.boccaccini@fau.de (A.R. Boccaccini).

https://doi.org/10.1016/j.oceram.2023.100413
Received 19 April 2023; Received in revised form 30 June 2023; Accepted 11 July 2023
Available online 17 July 2023

the limited interdiffusion in some complex silicates may impair the phase purity of the product. To overcome this difficulty, silicone-based mixtures may comprise additional fillers, not specifically reacting with silica but enhancing the interdiffusion, by forming an extra liquid phase upon ceramic conversion. As an example, in the case of åkermanite ceramic foams, borax (hydrated sodium borate, $Na_2B_4O_7{\cdot}10H_2O$) has been introduced as a 'multifunctional' filler [17], since it releases a significant amount of water vapour causing foaming at a low temperature, and sodium borate liquid phase at higher temperatures. In the presence of a liquid phase, pure åkermanite can be synthesized by using microparticles of the CaO and MgO precursors instead of nano-particles, i.e. under the conditions of relatively 'coarse' mixing of the constituents [17]. Since the liquid phase transforms into glass upon cooling, the obtained polymer-derived products resemble glass-ceramics (typically obtained by controlled crystallization of a parent glass) [10]. In other words, they may configure 'polymer-derived glass-ceramics'.

So far, limited attention has been dedicated to the biological response of polymer-derived ceramics. Promising results were previously achieved, in the CaO–MgO–SiO_2-based system, only with polymer-derived ceramic foams, developed by the addition of borax [18]. A relatively high concentration of boron oxide in the intergranular glass phase may represent a potential problem, considering the controversial findings related to borate bioactive glasses. In fact, boron is potentially toxic if released into the solution in the form of borate ions $(BO_3)^{3-}$ [19,20]. Some reports conclude that the toxic effects are concentration dependent: as an example, the borate bioactive glass 13–93B3 showed toxic effect onto murine MLO-A5 osteogenic cells *in-vitro* above the boron threshold concentration of 0.65 mmol L^{-1} in the cell culture medium. However, it supported cell proliferation and growth below that threshold [21]. Scaffolds based on the same glass did not exhibit any toxicity to cells *in-vitro* and supported new tissue infiltration when implanted in rats [22,23]. Other works on boron-containing glasses confirmed their bioactivity and biocompatibility [24,25]. The addition of borax, already known as additive for åkermanite-yielding silicone-based pastes, used for the direct ink writing of 3D scaffolds [14], has yet to be verified.

Phosphates represent an alternative to borate salts in polymer-derived glass-ceramics [10,26]. The addition of phosphorus appears as beneficial, considering that favorable cell response and rapid bone formation in many bioactive glasses is related to the release of Ca and P ions [27,28]. Except for some preliminary data on wollastonite-diopside foams, also P_2O_5-added polymer-derived bioceramics are yet to be explored in terms of biological response.

The present study is aimed at elucidating possible differences in terms of (*in vitro*) biomineralization (in simulated body fluid, SBF), cell viability (considering ST-2 cells) and antibacterial activity (against *S. aureus* and *E. coli*) of 'polymer-derived åkermanite glass-ceramics', studied in the form of 3D printed scaffolds, and related to the addition of borates or phosphates as active fillers. The obtained favorable results are intended to support preceramic polymers as reliable feedstock for silicate bioceramics.

2. Experimental procedure

2.1. Starting materials

A commercial silicone polymer (SILRES® MK, produced by Wacker Chemie AG, Munich, Germany) was used as the main silica source (it is known that 1 g of MK yields 0.84 g of amorphous silica, after firing in air at 1000 °C) [10]. The overall SiO_2 content was integrated by nano-sized fumed silica (FS, 7 nm, BET surface area of 220–280 m^2/g, Aerosil R106; Evonik, Essen Germany). Calcium carbonate ($CaCO_3$, Industries Bitossi, Vinci, Italy) and magnesium hydroxide ($Mg(OH)_2$, Sigma-Aldrich, Germany) were used as active fillers. Di-sodium hydrogen phosphate dodecahydrate ($Na_2HPO_4{\cdot}12H_2O$, Sigma-Aldrich, Germany) or borax ($Na_2B_4O_7{\cdot}10H_2O$, Sigma-Aldrich, Germany) were used as additional components.

Table 1
Batch formulations for åkermanite scaffolds with borax and di-sodium hydrogen phosphate (amounts of precursors in grams required to obtain 10 g of final ceramic product).[a,b]

Sample	Silicon Resin (MK Silres)	Fumed Silica (FS)	$CaCO_3$	$Mg(OH)_2$	IPA	Salt
Aker-B	4.72	0.44	7.33	2.14	3.1	0.3
Aker-P	4.72	0.44	7.33	2.14	3.1	0.5

[a] Aker-B contains 3 wt% of borax related to the total ceramic yield.
[b] Aker-P contains 5 wt% of hydrous sodium phosphate related to the total ceramic yield.

2.2. Direct ink writing of åkermanite scaffolds

Powdered MK silicone was first dissolved in isopropyl alcohol (IPA) and then added with FS (in the weight proportion MK:FS = 91.3:9.7, so that 90 wt% of the total silica was provided by the oxidation of MK and 10 wt% derived from FS) [10]. Then, $Mg(OH)_2$, $CaCO_3$ and di-sodium hydrogen phosphate ($Na_2HPO_4{\cdot}12H_2O$) or borax ($Na_2B_4O_7{\cdot}10H_2O$) active fillers were added, in the amounts shown in Table 1. The mixture was homogenized using a conditioning mixer (THINKY ARE-250, Thinky Co., Tokyo, Japan) for 2 min at a speed of 2000 min^{-1}. The obtained ink was transferred into a plastic syringe for direct ink writing (DIW). Scaffolds were printed layer-by-layer generating a 3D structure. Material was extruded in x- and y-dimension through a conical nozzle (Nordson EFD, Westlake, OH, USA), generating a diameter of 800 μm. The used Delta printer (Delta Wasp 2040 Turbo; WASP S. r.l., Massa Lombarda, Italy) was equipped with a pressurized vessel and an infinite screw paste extruder. After printing, the scaffolds were left at room temperature for one night to evaporate the solvent. As a final step the printed scaffolds were fired in air, following the stepwise heat treatment procedure: 80 °C for 5 h, 200 °C for 1 h, 550 °C for 3 h, 650 °C for 1 h, 800 °C for 3 h and finally 1100 °C for 3 h as described in reference [10].

2.3. Physical and mechanical properties

After heat treatment in air the dimensions of all samples were measured by a digital calliper. The apparent and true density of the obtained scaffolds were determined by a helium pycnometer (Micromeritics AccuPyc 1330, Norcross, GA). Microstructural characterization was performed by scanning electron microscopy (SEM, FEI Quanta 200 ESEM, Eindhoven, Netherlands), equipped with energy dispersive spectroscopy (EDS). The samples were subjected to compression tests (Quasar 25, Galdabini, Cardano, Italy), operating at a crosshead speed of 1 mm/min. Each data point represents an average value obtained by testing at least five specimens.

2.4. In vitro bioactivity

The *in vitro* bioactivity of 3D printed åkermanite scaffolds (Aker-B and Aker-P) derived from MK- silicone resin fired in air atmosphere was evaluated by immersion in SBF prepared according to Kokubo's method [29]. For the test, the sample (37.5 mg) was immersed in 70 mL of SBF and incubated under continuous agitation (120 rpm) at 37 °C for 1, 3, 7, 14, and 21 days. After each time interval, samples were collected and washed with deionized water to remove remaining SBF medium and dried overnight at 60 °C. The pH of the media was recorded after every time point. Finally, the samples were examined by scanning electron microscopy (SEM; Auriga Base, Zeiss) and Fourier Transform Infrared Spectroscopy (FTIR; IR Affinity- IS, Shimadzu) in attenuated total reflectance (ATR) mode, in a wavenumber range of 4000 to 400 cm^{-1} with a resolution of 4 cm^{-1} with 40 spectral scans. X-ray diffraction analysis using a diffractometer (XRD, Bruker AXS D8 Advance, Bruker,

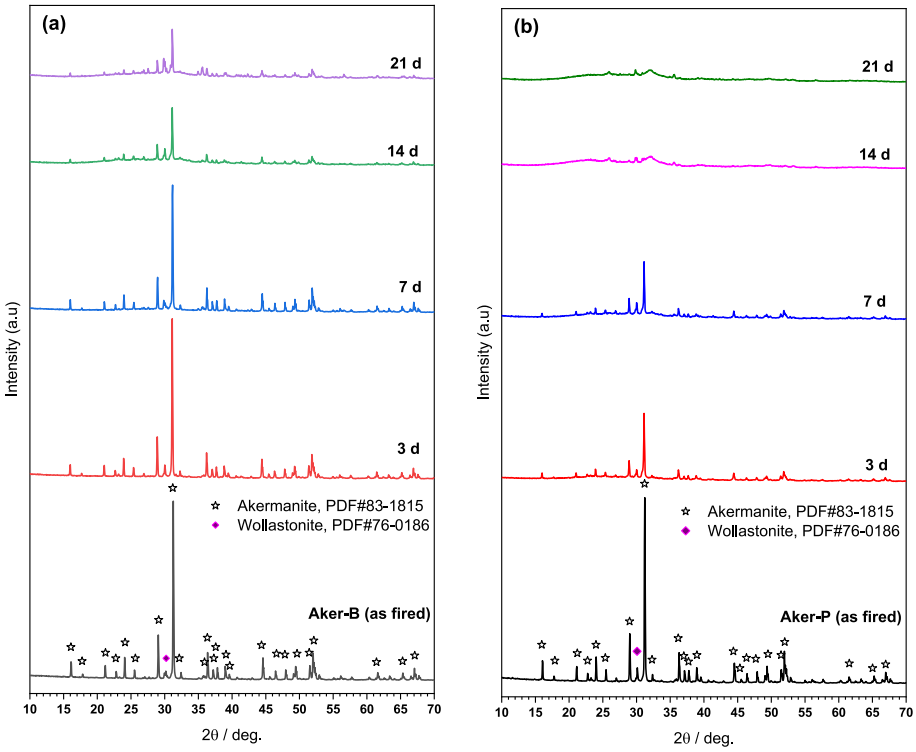

Fig. 1. X-ray diffraction patterns of Aker-B (a) and Aker-P (b) scaffolds after firing and after immersion in SBF for 3, 7, 14, and 21 days.

Germany) in the 2θ range of 10°–70° equipped with Cu Kα radiation was carried out to identify the phase composition after the immersion.

2.5. In vitro cell viability

Before starting cell viability experiments, Aker-B and Aker-P scaffolds were sterilized by heat treatment at 180 °C for 3 h in an electric oven (Nabertherm GmbH, Lilienthal, Germany). The samples with the weight of 0.2 g were then placed in 24 well plates and preconditioned for 7 days in cell culture medium RPMI 1640 (Gibco, Thermo Fisher Scientific Inc., MA, USA), containing 10 vol % of fetal bovine serum (FBS, Sigma-Aldrich), and 1 vol % of penicillin/streptomycin (Gibco). Direct contact cell viability approach was applied for both the Aker-B and Aker-P scaffolds using ST-2 stromal cells (Leibniz - Institut DSMZ - German Collection of Microorganisms and Cell Cultures GmbH, Braunschweig, Germany). This cell line was selected in analogy with previous experiences on the characterization of bioactive glasses [30]. Moreover, the ST-2 cells, as bone marrow-derived stroma cell line, showed the capability to differentiate in adipocytes, osteoblasts or chondrocytes and therefore they have been widely used in several tissue engineering applications, for hard and soft tissue regeneration and in studies for the assessment of angiogenesis [31–34].

The ST-2 cells were maintained in a cell culture medium at 37 °C in a humidified atmosphere of 95% air and 5% CO_2. ST-2 cell seeding was carried out directly on each printed sample with a 100 μL drop of cell suspension with an inoculum ratio of 5×10^4 cells/mL. Cell viability, after 1 day and 7 days incubation at 37 °C in 5% CO_2, was analysed by the WST-8 assay (CCK-8 Kit, Sigma Aldrich). Water-soluble tetrazolium salt, WST-8, is reduced by mitochondrial dehydrogenases to an orange formazan product. After incubation with 2% WST-8 reagent in the cell culture medium for 4 h at 37 °C, the reaction product was measured at 450 nm using a microplate reader (PHOmo Elisa reader, Autobio Diagnostics Co. Ltd.). The amount of formazan produced is directly proportional to the number of living cells in culture. The ST-2 cells cultured only with the cell culture medium were used as the positive control. WST-8 solution without cells was incubated at the same time and used as a blank.

Additionally, Rhodamine Phalloidin (RP; ThermoFisher Scientific) and DAPI (ThermoFisher Scientific) staining was performed to explore cell adhesion and morphology. The staining protocol started with fixation and permeabilization of the adherent cells. Afterwards, Rhodamine Phalloidin (8 μL/mL) was added and incubated at 37 °C for 1 h. Incubated samples were rinsed gently with PBS and dyed by DAPI (1 μL/mL) for 5 min. A fluorescent microscope (Axio Scope A1, Zeiss) was used for the analysis. Each experiment was carried out in triplicate.

2.6. Antibacterial activity

The antibacterial activity of Aker-B and Aker-P scaffolds was separately tested with *S. aureus* (Gram-positive) and *E. coli* (Gram-negative) bacteria. The bacterial suspensions were prepared for both bacteria strains in lysogeny broth medium (LB medium) at 37 °C for 24 h. The optical density (OD) (600 nm, Thermo Scientific GENESYS 30, Germany) of the cultivated bacteria was set at 0.015 according to turbidity measurements of bacterial cultures. Prior to the evaluation of the antibacterial activity, the Aker-B and Aker-P scaffolds were sterilized at 180 °C for 3 h. 0.2 g of sterilized scaffolds was added to 2 mL LB medium (without bacteria) and were placed into a falcon tube (15 mL) incubated for 24 h by continuous shaking. After the scaffold separation from the LB medium, the bacterial suspension with a volume of 20 μL was added. The samples were incubated at 37 °C for predetermined times (3, 6, and 24 h). At the given time-points, aliquots of bacterial suspension were taken out, and their optical density was recorded and relative bacterial viability was calculated as follows:

$$\text{Relative Bacterial Viability } (\%) = \frac{\text{Sample OD}}{\text{Control OD}} \times 100 \quad (1)$$

The lysogeny broth medium and bacterial cell suspension in lysogeny broth medium were used as a blank and control, respectively. The experiments were made in triplicate.

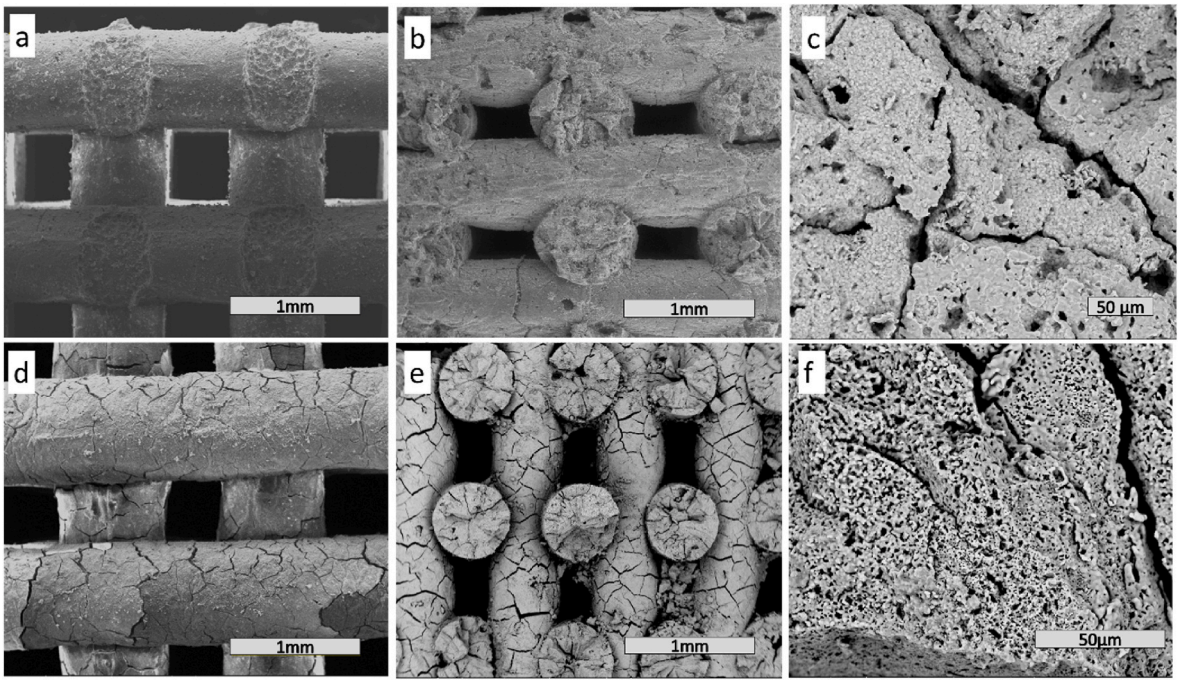

Fig. 2. SEM images of 3D printed and fired scaffolds, a; top view b; cross section and c; struts of Aker-B, and d; top view e; cross section, f; struts Aker-P scaffolds.

Table 2
Physical and mechanical properties of 3D printed Aker-B and Aker-P scaffolds.

Sample Name	Geometrical density ρ (g/cm^3)	Open porosity (%)	Total porosity, % [$\rho_{rel} = 1\text{-}P_{tot}$]	Compressive strength ($\sigma_{c)}$, (MPa) [σ_{bend} (MPa)]
Aker-B	1.01 ± 0.05	70.8 ± 0.2	71.0 ± 0.1 m [ρ_{rel}: 0.29]	4.1 ± 0.4 [131.3]
Aker-P	0.84 ± 0.06	72.6 ± 0.2	73.1 ± 0.1 [ρ_{rel}: 0.27]	2.2 ± 0.2 [78.4]

2.7. Statistical analysis

All experiments were carried out at least in triplicate. Results are expressed as the mean ± standard deviation (SD). Statistical evaluation was assessed by using one-way analysis of variance (ANOVA) with $p < 0.05$ considered significant.

3. Results and discussions

3.1. Microstructural properties of 3D printed åkermanite scaffolds

Fig. 1 shows that both Aker-B and Aker-P formulations yielded nearly the pure phase åkermanite. All diffraction maxima match the theoretical pattern of the crystal ($Ca_2MgSi_2O_7$, PDF#83-1815), except for the low intensity maxima at 2θ~30°, attributable to minor wollastonite (β-$CaSiO_3$, PDF#76-0186) contamination.

For Aker-B scaffolds, nearly phase pure åkermanite was developed by duplicating a formulation proposed earlier [14], in which borax was added in the amount of 3 wt% of the total ceramic yield of other reactants. Concerning Aker-P, to the best of our knowledge, there are no previous reports on adopting a phosphate filler in the development of åkermanite ceramics. Di-sodium hydrogen phosphate was proposed in analogy to previous experiments on wollastonite-diopside system [35], and it was applied in variable amounts (not shown). The amount presented here (5 wt% of the total ceramic yield of other reactants) represents the minimum required for the development of åkermanite not accompanied by other undesired phases.

Compared to previous experiments [14], the scaffolds were intentionally printed with larger struts (~0.8 mm, instead of ~0.4 mm), as shown by Fig. 2, to favour subsequent cell seeding experiments. This choice did not compromise the integrity of Aker-B (Fig. 2a and b), but determined some changes in the cross-section. The scaffolds reported in Ref. [14] exhibited a homogeneous spongy-like cross-section, not visible in Fig. 2c. We supposed that the enhanced stiffness of the structure with thicker struts could hinder the viscous flow of the liquid phase and impede uniform foaming. However such changes did not affect the strength of Aker-B samples, shown in Table 2. Compressive strength data of highly porous ceramics are usually difficult to interpret due to the variability of overall porosity and pore distribution. However, the Gibson-Ashby model offers a simplified tool [36]. Based on this model, the compressive strength (σ_c) is a function of relative density (ρ_{rel}) and bending strength (σ_{bend}) of the solid phase: $\sigma_c \cong 0.2 \cdot \sigma_{bend} \cdot (\rho_{rel})^{1.5}$

From the experimental data of compressive strength and relative density, the σ_{bend} values fitting the equation cannot be considered as a real attribute of the material, but an expression of the integrity of a sample. The calculated σ_{bend} of ~130 MPa of Aker-B matches well the values for similar scaffolds discussed previously [14] and the data for dense åkermanite ceramics [37]. The reduction to ~80 MPa is acceptable for Aker-P, considering the significant cracking (Fig. 2d and e). In this case, the struts revealed a spongy, foamed cross-section (Fig. 2f).

3.2. In vitro biomineralization

X-ray diffraction, infrared spectroscopy and scanning electron microscopy were used to assess the deposition of hydroxycarbonate apatite (HCA) on the surface of fabricated scaffolds after immersion in SBF for 1, 3, 7, 14, and 21 days. Fig. 1 displays also the evolution of patterns of Aker-B and Aker-P scaffolds soaked in SBF for different times, for 3, 7, 14, and 21 days. The patterns on day 1 are not shown since they did not show any difference from the as-prepared state.

For the Aker-B scaffold the intensity of åkermanite diffraction maxima decreased substantially only after 14 days of immersion in SBF (Fig. 1). On the contrary, the Aker-P scaffolds exhibited a fast dissolution, with åkermanite diffraction maxima reduced already after 3 days of immersion. After 14 days of immersion in SBF the scaffold was completely dissolved.

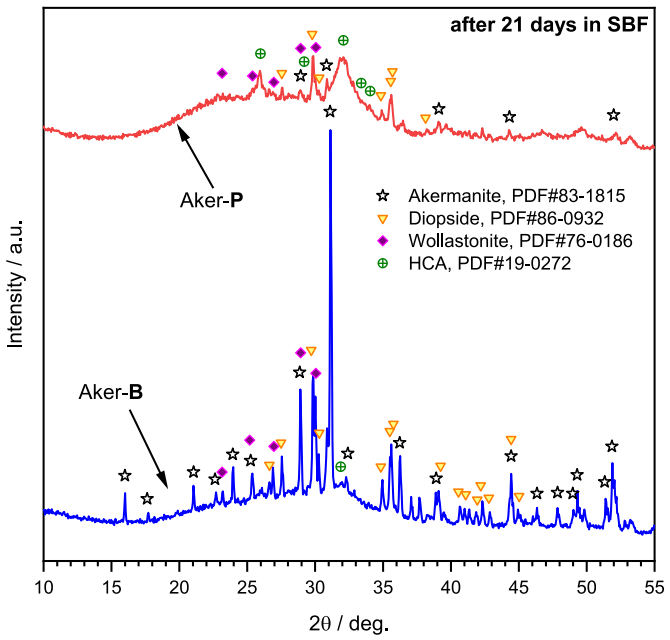

Fig. 3. A comparison of X-ray diffraction patterns of Aker-P and Aker-B scaffolds after immersion in SBF for 21 days.

A direct comparison of the XRD patterns of Aker-B and Aker-P scaffolds after immersing in SBF solution for 21 days is shown in Fig. 3. The absence of a flat background indicates the formation of an amorphous phase; small, flattened additional diffraction maxima are consistent with the formation of HCA ($Ca_{10}(PO_4)_3(CO_3)_3(OH)_2$, PDF#19-0272) nano-crystals, especially for Aker-P. Unexpectedly, some peaks could further be attributed to diopside ($CaMgSi_2O_6$, PDF#86-0932). In our opinion, these diffraction maxima do not represent a newly formed phase, but they may be a result of dissolution of the starting material. Diopside, as well as wollastonite, could be present in the as fired material, as an impurity of åkermanite (diopside, compared to åkermanite contains the same oxides - CaO, MgO and SiO_2 -, but at different proportions). The dissolution of åkermanite likely concentrated the impurities, making them more visible by diffraction.

Infrared spectroscopy provided additional information concerning the evolution of Aker-B and Aker-P scaffolds after exposure to SBF. Fig. 4 shows the FTIR spectra of Aker-B and Aker-P scaffolds after immersion in the SBF for 1, 3, 7, 14, and 21 days. The FTIR spectrum of the unreacted åkermanite samples exhibited vibration bands (labelled as A), in the same positions as reported in literature for åkermanite [38], which persisted despite the observed amorphization at long immersion times, probably due to the progressive appearance of diopside. The FTIR spectrum of Aker-P scaffolds after 21 days immersion in SBF contained two bands at 567 cm^{-1}, corresponding to P–O υ_4 bending vibrations, and at 1060 cm^{-1}, corresponding to the P–O υ_3 stretching vibrations. These are regarded as the evidence for the growth of hydroxycarbonate apatite [39]. For Aker-B scaffolds, the P–O stretching vibration band at 567 cm^{-1} was missing after 21 days immersion, suggesting an amorphous deposit [40].

The SEM images of Aker-B and Aker-P soaked in SBF for 21 days are presented in Fig. 5. The surface of both scaffolds before soaking showed a smooth morphology (Fig. 2). After the exposure, the sample surface was covered by tiny particles with rounded morphology, attributed to phosphatization reactions [41]. It should be noted that Aker-B did not contain any source of phosphorus. However, the energy dispersive X-ray spectroscopy measurements detected phosphorus, and a Ca/P ratio of ~ 1.67 was determined after immersion in SBF for 21 days. The Ca/P ratio of 1.67 is characteristic for calcium-phosphate-based bio-ceramics that forms a mechanically strong bond to bone [42].

Apatite nucleation is known to depend on the presence of sites, such as silanol (Si–OH) groups, favoring the attachment of apatite components [33]. These groups are abundant in hydrated silica gel layers, formed upon ion exchange between cations in the silicate and H_3O^+ from the solution, and documented by an increase in the solution pH. In

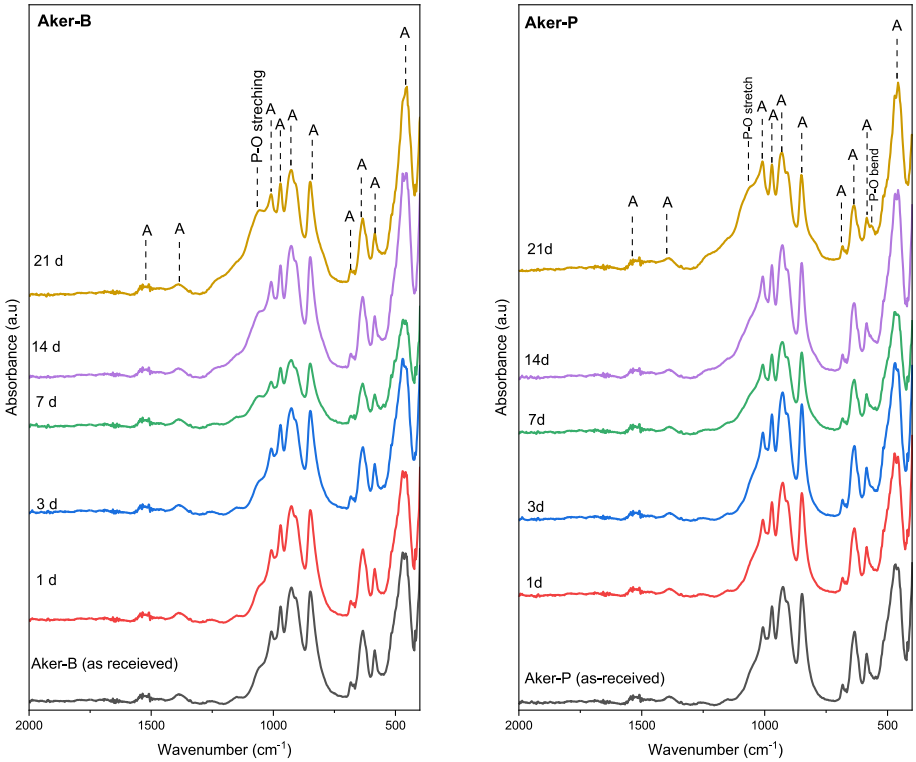

Fig. 4. FTIR spectra of Aker-B and Aker-P scaffolds after immersion in SBF for 1, 3, 7, 14, and 21 days.

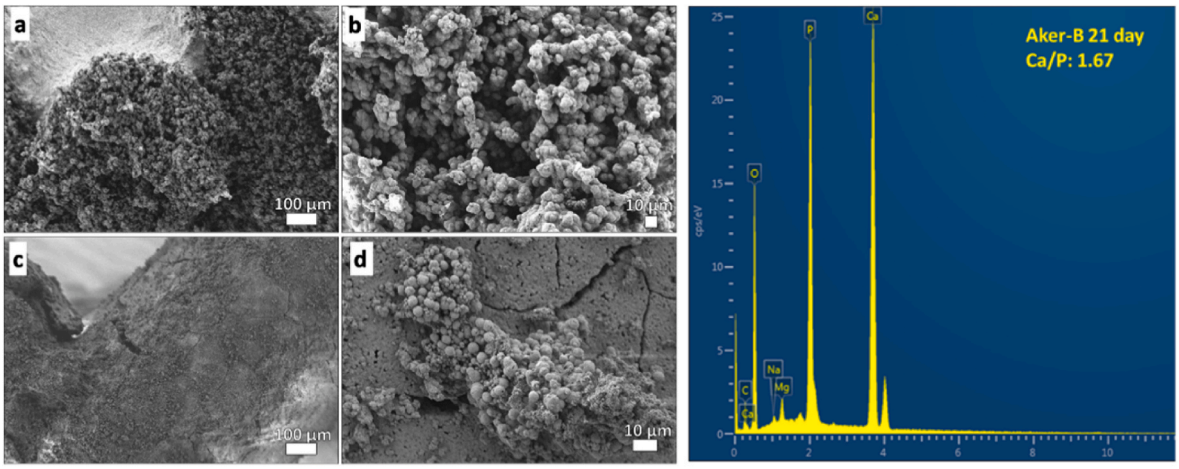

Fig. 5. left) SEM images of åkermanite scaffolds soaked in SBF for 21 days: a,b) Aker-B (high magnification), c,d) Aker-P; right) EDX spectrum of Aker-B scaffold after immersion in SBF for 21 days.

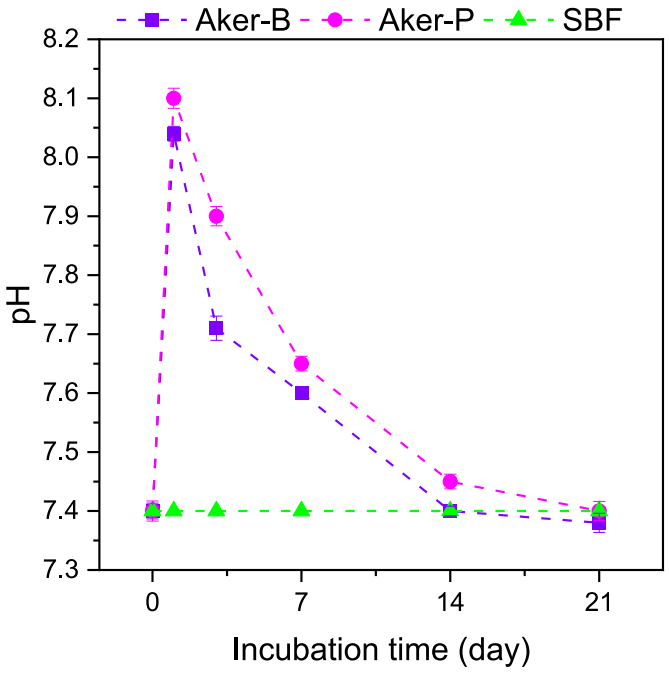

Fig. 6. pH values of Aker-B and Aker-P scaffolds in SBF after 1, 3, 7, 14, and 21 days.

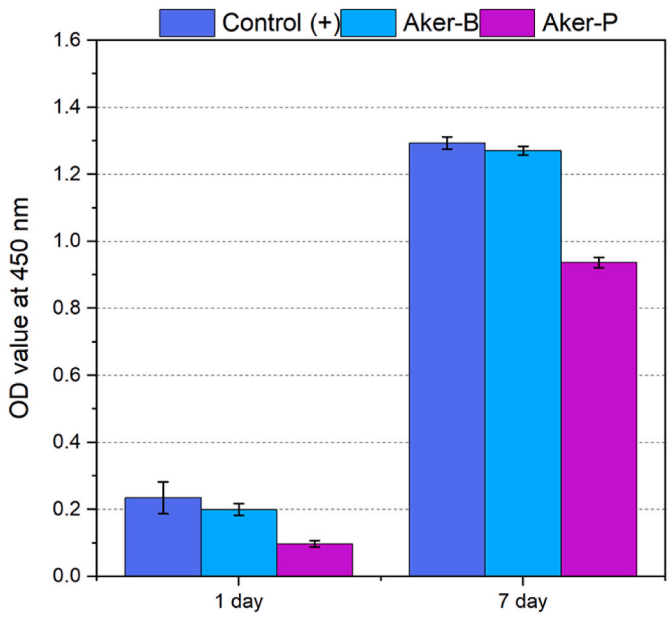

Fig. 7. Cell viability (by WST-8 assay) results of ST-2 cells on MK-derived åkermanite scaffolds (5×10^4 cell/piece (in the drop of 100 µL)), after 7 days preconditioning (n = 3, samples in triplicate).

addition, water molecules in SBF react with the Si–O–Si groups to create additional Si–OH groups [43].

Ion exchange was documented also for Aker-B and Aker-P scaffolds. The solution pH increased from 7.4 to 8.05 for Aker-B and to 8.10 for Aker-P scaffolds (Fig. 6). A gradual decrease of the pH down to initial values after 14–21 days of immersion is attributed to the specific role of Ca^{2+} ions absorbing phosphate groups from the solution. The relatively slow recovery of the initial pH value is attributed to the presence of Mg^{2+} ions, strongly bonded in the crystal structure of åkermanite (Ca^{2+} ions are sandwiched between Mg-silicate infinite sheets) [44].

3.3. *In vitro cell viability*

Both Aker-B or Aker-P exhibited improved cell viability results after 7 days preconditioning in cell culture medium in relation to the results obtained after 1 day (Fig. 7). From the values of the optical density (OD) at 450 nm, it is possible to conclude that comparable values have been obtained for the two samples at both incubation time points, demonstrating that preconditioning step for 7 days contributed to the ST-2 cell viability on the Aker-B and Aker-P scaffolds due to the stabilized pH/ion release in cell culture media. Moreover, cell proliferation for both samples can be evaluated considering the ratio obtained by dividing the average OD value at the time point d_7 by the same value at d_1. These ratios are 5.5 for control, 6.38 for Aker-B and 9.63 for Aker-P. This result shows that the produced polymer-derived åkermanite ceramics are comparable, in terms of cell proliferation, to åkermanite ceramics produced by conventional methods: as an example, åkermanite extract had three-fold increase of viability of bone marrow mesenchymal stem cells (MSCs) [45]. In addition, Mg ions significantly enhance osteoblast adhesion [46], and directly stimulate osteoblast proliferation with a comparative effect to insulin which is known as a growth factor for osteoblasts [47]. Wu et al. [48] showed that osteoblasts spread very well on the surface of åkermanite ceramics and proliferated with increasing culture time.

Fluorescence microscopy images of both samples are correlated with

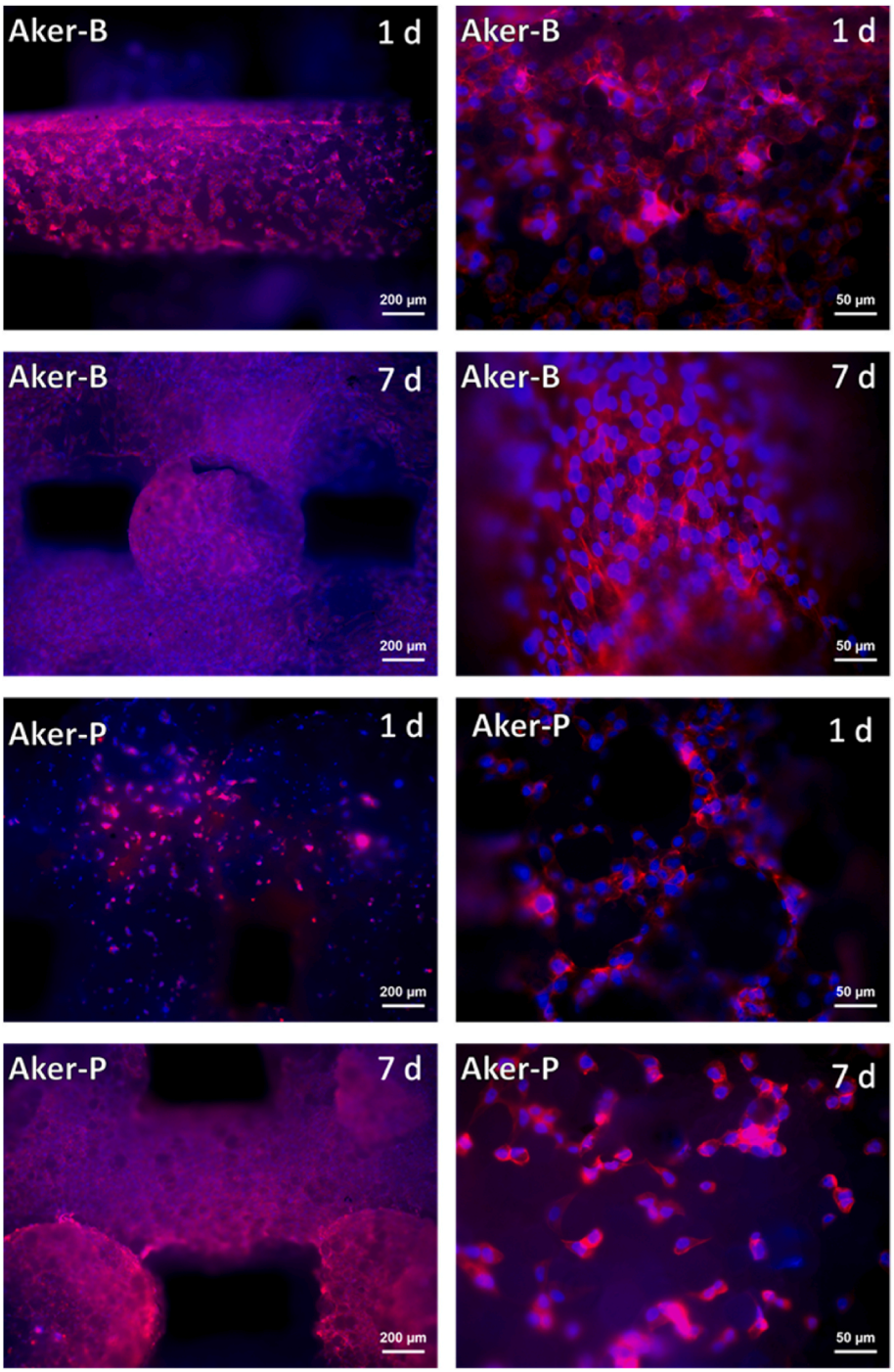

Fig. 8. Fluorescence microscopy images at different magnifications of preconditioned Aker-B and Aker-P scaffolds after 1 day and 7 days cell seeding. Cell nuclei (blue, DAPI) and cytoskeleton (red, rhodamine phalloidin) of ST-2 cells on the åkermanite scaffolds.

the cell viability results of ST-2 cells. The characteristic cellular morphology, visualized by fluorescent staining of nuclei and cells seeded on the scaffolds, is visible in Fig. 8. Actin filaments related to migration and cell-cell interactions became strongly visible particularly for the Aker-P scaffolds. Based on the obtained results, the åkermanite scaffolds are considered cytocompatible and can support cell adhesion [49].

3.4. Antibacterial activity

The antibacterial activity of the synthesized åkermanite scaffolds was studied both against Gram-negative (*E. coli*) and Gram-positive (*S. aureus*) bacteria for 3, 6, and 24 h. The results are shown in Fig. 9a and b, respectively, based on the relative bacteria viability (%). It should be pointed out that relative bacteria viability slightly increased in the Aker-B scaffold for the first 3 h for both *E. coli and S. aureus*. Later on, it decreased for both types of bacteria with the increasing incubation time for all samples.

The relative bacteria viability for both Aker-B and Aker-P scaffolds after 24 h of incubation, was lower for *S. aureus* than for *E. coli*. This can be attributed to inherent features of the bacteria. In particular, *E. coli* has an outer plasma membrane with a thicker lipopolysaccharide layer. This, compared to the peptidoglycan layer in *S. aureus*, makes it more resistant even to antibiotics [50].

In general, the main reason for the antibacterial effect of bioceramics

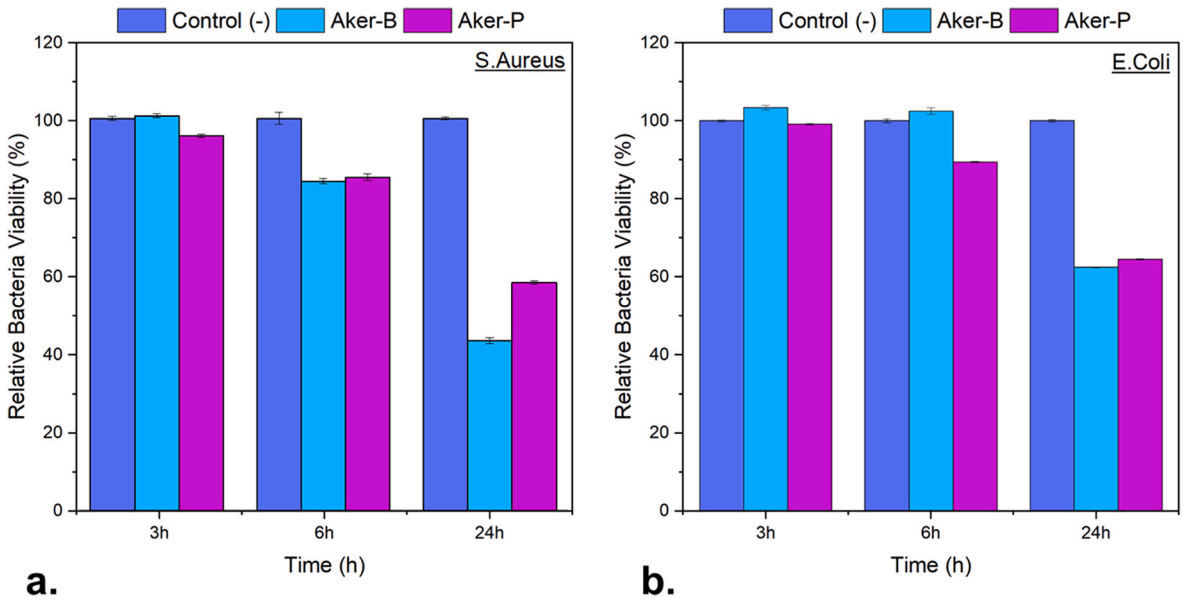

Fig. 9. Antibacterial activity of MK-derived Aker-P and Aker-B scaffolds after 3, 6, and 24 h incubation with a) S. aureus (Gram-positive) and b) E. coli (Gram-negative) bacteria (n = 3, samples in triplicate).

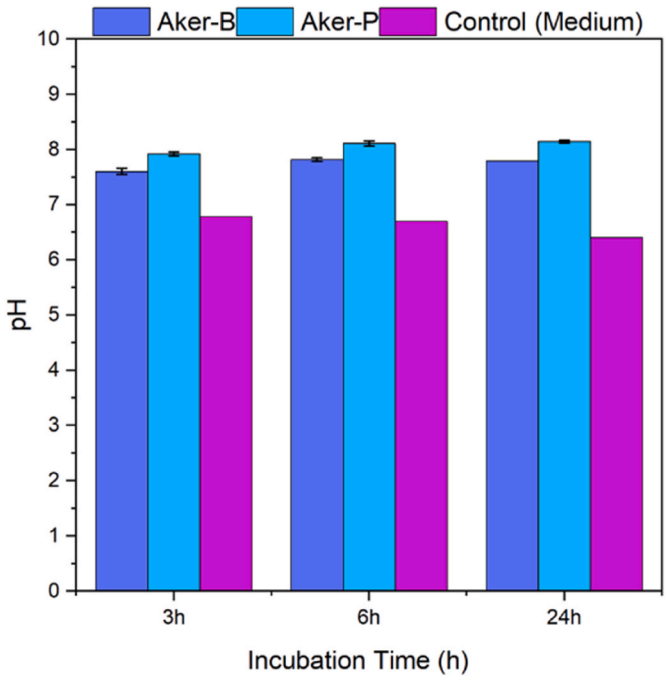

Fig. 10. pH changes in LB medium (0.2 g scaffold: 2 mL medium) after 3, 6, and 24 h of incubation (n = 3, samples in triplicate).

is their ability to induce a localized increase of pH value in the media in which they are immersed [3,51]. Fig. 10 indicates that the pH increased already after 3 h immersion in LB medium, followed by a decrease after 1 day, as indicated by the results from SBF shown in Fig. 6. The obtained levels do not favour bacteria survival and proliferation [3,52,53]. Again, the results for polymer-derived åkermanite ceramics confirmed and further extended previous findings on similar materials prepared by conventional methods. For example, Collin et al. [3] reported antibacterial activity of åkermanite only against *S. aureus,* while diopside and merwinite samples possessed antibacterial activity both against *E. coli* and *S. aureus*.

In conclusion, the biological response of polymer-derived åkermanite ceramics, independently from the 'flux' (i.e. provider of liquid phase, upon heat treatment), is consistent with that of ceramics featuring the same main phase. This is a fundamental point, besides the easiness of application of additive manufacturing and direct synthesis (i.e. direct firing of printed pastes instead of processing of previously-prepared åkermanite powders [2,3]), to establish silicone and reactive fillers as feedstock for bioceramics, although additional efforts are expected, in order to provide a 'quantitative' comparison between polymer-derived ceramics and those from conventional technologies. Further tuning opportunities are envisaged, according to the transformation of silicones not only in air, into silica, but also in nitrogen, into silica (reacting with fillers) and carbon (as inert, extra phase) [12]. Silicate/carbon composites will be the specific object of future studies.

4. Conclusions

Reticulated åkermanite ceramics-based scaffolds were prepared from silicone-based mixtures and Mg and Ca salts used as active fillers. Sodium phosphate was used as an alternative to sodium borate, as a source of liquid phase during firing at 1100 °C. The use of sodium phosphate impaired the structural integrity of scaffolds, resulting in substantial micro-cracking of the samples, but it did not affect the biological response. Within the studied concentration range, the *in-vitro* bioactivity and cytocompatibility were confirmed also for B_2O_3-containing scaffolds (Aker-B). Under the applied cell culture conditions, both borate- and phosphate-added åkermanite (Aker-B and Aker-P) ceramics were cytocompatible with the ST-2 cell line, and exhibited antibacterial effect against *S. aureus* and *E. coli* bacteria.

Declaration of competing interests

The authors declare that they have no known competing financial interests or personal relationships that could have appeared to influence the work reported in this paper.

Acknowledgments

This paper is a part of the dissemination activities of project FunGlass. This project has received funding from the European Union's Horizon 2020 research and innovation program under grant agreement

No 739566. The financial support of this work by the grants APVV-19-0010 and SAS-MOST JRP 2018/02 are gratefully acknowledged. Helpful discussions with Dr Irem Unalan (Institute of Biomaterials, FAU) are appreciated.

References

[1] W. Zhai, H. Lu, C. Wu, L. Chen, X. Lin, K. Naoki, G. Chen, J. Chang, Stimulatory effects of the ionic products from Ca–Mg–Si bioceramics on both osteogenesis and angiogenesis in vitro, Acta Biomat 9 (2013) 8004–8014, https://doi.org/10.1016/j.actbio.2013.04.024.

[2] A. Liu, M. Sun, X. Yang, C. Ma, Y. Liu, X. Yang, S. Yan, Z. Gou, Three-dimensional printing akermanite porous scaffolds for load-bearing bone defect repair: an investigation of osteogenic capability and mechanical evolution, J. Biomater. Appl. 31 (2016) 650–660, https://doi.org/10.1177/0885328216664839.

[3] M.S. Collin, S.K. Venkatraman, M. Sriramulu, S. Shanmugam, E.A. Drweesh, M. M. Elnagar, E.S. Mosa, S. Sasikumar, Solution combustion synthesis of functional diopside, akermanite, and merwinite bioceramics: excellent biomineralization, mechanical strength, and antibacterial ability, Mater. Today Commun. 27 (2021), 102365, https://doi.org/10.1016/j.mtcomm.2021.102365.

[4] P. Zadehnajar, M.H. Mirmusavi, S.S. Eil Bakhtiari, H.R. Bakhsheshi-Rad, S. Karbasi, S.R. Krishna, F. Berto, Recent advances on akermanite calcium-silicate ceramic for biomedical applications, Int. National of Appl. Ceram. Tech. 6 (2021) 1901–1920.

[5] S. Hu, C. Ning, Y. Zhou, L. Chen, K. Lin, J. Chang, Antibacterial activity of silicate bioceramics, Journal of Wuhan University of Technology-Mater. Sci 26 (2011) 226–230, https://doi.org/10.1007/s11595-011-0202-8.

[6] X. Dong, H. Li, L. E, J. Cao, B. Guo, Bioceramic akermanite enhanced vascularization and osteogenic differentiation of human induced pluripotent stem cells in 3D scaffolds in vitro and vivo, RSC Adv. 9 (2019) 25462–25470, https://doi.org/10.1039/C9RA02026H.

[7] A. Francis, R. Detsch, A.R. Boccaccini, Fabrication and cytotoxicity assessment of novel polysiloxane/bioactive glass films for biomedical applications, Ceram. Int. 42 (2016) 15442–15448, https://doi.org/10.1016/j.ceramint.2016.06.195.

[8] X. Fangtong, I. Gonzalo-Juan, H. Breitzke, C. Fasel, M. Trapp, G. Buntkowsky, H. Kleebe, R. Riedel, A.R. Boccaccini, E. Ionescu, Effect of Ca and B incorporation into silicon oxycarbide on its microstructure and phase composition, J. Am. Ceram. Soc. 102 (2019) 7645–7655, https://doi.org/10.1111/jace.16620.

[9] A. Francis, Biological evaluation of preceramic organosilicon polymers for various healthcare and biomedical engineering applications: a review, J. Biomed. Mater. Res., Part B 109 (2021) 744–764, https://doi.org/10.1002/jbm.b.34740.

[10] H. Elsayed, P. Rebesan, M.C. Crovace, E.D. Zanotto, P. Colombo, E. Bernardo, Biosilicate® scaffolds produced by 3D-printing and direct foaming using preceramic polymers, J. Am. Ceram. Soc. 102 (2019) 1010–1020, https://doi.org/10.1111/jace.15948.

[11] P. Colombo, G. Mera, R. Riedel, G.D. Sorarù, Polymer-derived ceramics: 40 Years of research and innovation in advanced ceramics, J. Am. Ceram. Soc. 93 (2010) 1805–1837, https://doi.org/10.1111/j.1551-2916.2010.03876.x.

[12] F. Dogrul, S. Bortolin, D. Del Col, N. Dengo, D. Pedron, M. Michalek, H. Elsayed, D. Galusek, E. Bernardo, Polymer-derived Biosilicate-C composite foams: phase development and photothermal effect, J. Eur. Ceram. Soc. 41 (2021) 380–388, https://doi.org/10.1016/j.jeurceramsoc.2021.09.012.

[13] E. Bernardo, P. Colombo, E. Dainese, G. Lucchetta, P.F. Bariani, Novel 3D wollastonite-based scaffolds from preceramic polymers containing micro- and nano-sized reactive particles, Adv. Eng. Mater. 4 (2012) 269–274.

[14] A. Dasan, H. Elsayed, J. Kraxner, D. Galusek, E. Bernardo, Hierarchically porous 3D-printed akermanite scaffolds from silicones and engineered fillers, J. Eur. Ceram. Soc. 39 (2019) 4445–4449.

[15] F. Dogrul, P. Ożóg, M. Michálek, H. Elsayed, D. Galusek, L. Liverani, A. R. Boccaccini, E. Bernardo, Polymer-derived biosilicate®-like glass-ceramics: engineering of formulations and additive manufacturing of three-dimensional scaffolds, Materials 14 (2021) 5170, https://doi.org/10.3390/ma14185170.

[16] A. Dasan, H. Elsayed, J. Kraxner, D. Galusek, P. Colombo, E. Bernardo, Engineering of silicone-based mixtures for the digital light processing of Åkermanite scaffolds, J. Eur. Ceram. Soc. 40 (2020) 2566–2572, https://doi.org/10.1016/j.jeurceramsoc.2019.11.087.

[17] E. Bernardo, J. Carlotti, P.M. Dias, L. Fiocco, P. Colombo, L. Treccani, U. Hess, K. Rezwan, Novel akermanite-based bioceramics from preceramic polymers and oxide fillers, Ceram. Int. 40 (2014) 1029–1035, https://doi.org/10.1016/j.ceramint.2013.06.100.

[18] L. Fiocco, S. Li, M.M. Stevens, E. Bernardo, J.R. Jones, Biocompatibility and bioactivity of porous polymer-derived Ca-Mg silicate ceramics, Acta Biomater. 50 (2017) 56–67, https://doi.org/10.1016/j.actbio.2016.12.043.

[19] M.N. Rahaman, D.E. Day, B. S Bal, Q. Fu, S.B. Jung, L.F. Bonewald, A.P. Tomsia, Bioactive glass in tissue engineering, Acta Biomater. 7 (2001) 2355–2373.

[20] A. Hoppe, N. S Güldal, A.R. Boccaccini, A review of the biological response to ionic dissolution products from bioactive glasses and glass-ceramics, Biomaterials 32 (2011) 2757–2774.

[21] Q. Fu, E. Saiz, M. N Rahaman, A.P. Tomsia, Bioactive glass scaffolds for bone tissue engineering: state of the art and future perspectives, Mater. Sci. Eng. C 31 (2011) 1245–1256.

[22] F. Baino, C. Vitale-Brovarone, Three-dimensional glass-derived scaffolds for bone tissue engineering: current trends and forecasts for the future, J. Biomed. Mater. Res, Vol. A 97 (2011) 514–535.

[23] A.A. Gorustovich, J.M.P. Lopez, M.B. Guglielmotti, R.L. Cabrini, Biologic performance of boron-modified bioactive glass particles implanted in rat tibia bone marrow, Biomed. Mater. 1 (2006) 100–105.

[24] G. Kaur, G. Pickrell, G. Kimsawatde, D. Homa, H.A. Allbee, N. Sriranganathan, Synthesis cytotoxicity, and hydroxypatite formation in 27-Tris-SBF for sol-gel based CaO-P_2O_5-SiO_2-B_2O_3-ZnO bioactive glasses, Sci. Rep. 4 (2014) 1–14.

[25] M.N. Rahaman, W. Liang, D.E. Day, N.W. Marion, G.C. Reilly, J. J Mao, Bioactive characteristics of porous borate glass substrates, Ceram. Eng. Sci. Proc. 26 (2005) 3–10.

[26] L. Fiocco, H. Elsayed, L. Ferroni, C. Gardin, B. Zavan, E. Bernardo, Bioactive wollastonite-diopside foams from preceramic polymers and reactive oxide fillers, Materials 8 (2015) 2480–2494.

[27] S.M. Best, A.E. Porter, E.S. Thian, J. Huang, Bioceramics: past, present and for the future, J. Eur. Ceram. 28 (2008) 1319–1327.

[28] I.D. Xynos, A.J. Edgar, L.D. Buttery, L.L. Hench, J.M. Polak, Gene-expression profiling of human osteoblasts following treatment with the ionic products of Bioglass 45S5 dissolution, J. Biomed. Mater. Res. 55 (2001) 151–157.

[29] T. Kokubo, H. Takadama, How useful is SBF in predicting in vivo bone bioactivity? Biomaterials 27 (2006) 2907–2915, https://doi.org/10.1016/j.biomaterials.2006.01.017.

[30] V. Miguez-Pacheco, D. de Ligny, J. Schmidt, R. Detsch, A.R. Boccaccini, Development and characterization of niobium-releasing silicate bioactive glasses for tissue engineering applications, J. Eur. Ceram. Soc. 38 (2018) 871–876, https://doi.org/10.1016/j.jeurceramsoc.2017.07.028.

[31] J. Ding, K. Nagai, J. Woo, Insulin-dependent adipogenesis in stromal ST2 cells derived from murine bone marrow, Biosci. Biotechnol. Biochem. 67 (2003) 314–321, https://doi.org/10.1271/bbb.67.314.

[32] E. Otsuka, A. Yamaguchi, S. Hirose, H. Hagiwara, Characterization of osteoblastic differentiation of stromal cell line ST2 that is induced by ascorbic acid, Am. J. Physiol. 277 (1999) C132, https://doi.org/10.1152/ajpcell.1999.277.1.C132.–C138.

[33] J.C. Robins, N. Akeno, A. Mukherjee, R.R. Dalal, B.J. Aronow, P. Koopman, T. L. Clemens, Hypoxia induces chondrocyte-specific gene expression in mesenchymal cells in association with transcriptional activation of Sox9, Bone 37 (2005) 313–322, https://doi.org/10.1016/j.bone.2005.04.040.

[34] P. Balasubramanian, L. Hupa, B. Jokic, R. Detsch, A. Grünewald, A.R. Boccaccini, Angiogenic potential of boron-containing bioactive glasses: in vitro study, J. Mater. Sci. 52 (2017) 8785–8792, https://doi.org/10.1007/s10853-016-0563-7.

[35] L. Fiocco, H. Elsayed, J.K.M.F. Daguano, V.O. Soares, E. Bernardo, Silicone resins mixed with active oxide fillers and Ca–Mg silicate glass as alternative/integrative precursors for wollastonite-diopside glass-ceramics foams, J. Non-Cryst. Solids 416 (2015) 44–49.

[36] L.J. Gibson, M.G. Ashby, Cellular Solids, Structure and Properties, Cambridge University Press, Cambridge, UK, 1999.

[37] Z. Han, P. Feng, C. Gao, Y. Shen, C. Shuai, S. Peng, Microstructure, mechanical properties and in vitro bioactivity of akermanite scaffolds fabricated by laser sintering, Bio Med. Mater. Eng. 24 (2014) 2073–2080.

[38] J. Hanuzaab, M. Ptaka, M. Mączkaa, K. Hermanowicza, J. Lorencb, A.A. Kaminskii, Polarized IR and Raman spectra of $Ca_2MgSi_2O_7$, $Ca_2ZnSi_2O_7$ and $Sr_2MgSi_2O_7$ single crystals: temperature-dependent studies of commensurate to incommensurate and incommensurate to normal phase transitions, J. Solid State Chem. 191 (2012) 90–101.

[39] W.B. I Rehman, Characterization of hydroxylapatite and carbonated apatite by photo acoustic FTIR spectroscopy, J. Mater. Sci. Mater. Med. 8 (1997) 1–4.

[40] S.N. Danilchenko, A.N. Kalinkevich, R.A. Moskalenko, V.N. Kuznetsov, A. V. Kochenko, E.V. Husak, V.V. Starikov, F. Liu, J. Meng, J. Lü, Structural and crystal-chemical characteristics of the apatite deposits from human aortic walls, Interv Med Appl Sci 10 (2018) 10–119.

[41] L. Fiocco, B. Michielsen, E. Bernardo, Silica-bonded apatite scaffolds from calcite-filled preceramic polymers, J. Eur. Ceram. Soc. 36 (2016) 3211–3218, https://doi.org/10.1016/j.jeurceramsoc.2016.05.013.

[42] C.Y. Tan, R. Singh, Y.C. Teh, Y.M. Tan, The effects of calcium-to-phosphorus ratio on the densification, Int. J. Appl. Ceram. Technol. 12 (2014) 223–227.

[43] N.M. Alves, I.B. Leonor, H. S Azevedo, R.L. Reis, J.F. Mano, Designing biomaterials based on biomineralization of bone, J. Mater. Chem. 20 (2010) 2911–2921.

[44] I.P. Swainson, M.T. Dove, W.W. Schmahl, A. Putnis, Neutron powder diffraction study of the åkermanite-gehlenite solid solution series, Phys. Chem. Miner. 19 (1992) 185–195, https://doi.org/10.1007/BF00202107.

[45] L. Xia, Z. Yin, L. Mao, X. Wang, J. Liu, X. Jiang, Z. Zhang, K. Lin, J. Chang, B. Fang, Akermanite bioceramics promote osteogenesis, angiogenesis and suppress osteoclastogenesis for osteoporotic bone regeneration, Sci. Rep. 6 (2016), 22005, https://doi.org/10.1038/srep22005.

[46] T.J. Webster, C. Ergun, R.H. Doremus, R. Bizios, Hydroxylapatite with substituted magnesium, zinc, cadmium, and yttrium. II. Mechanisms of osteoblast adhesion, J. Biomed. Mater. Res. 59 (2002) 312–317, https://doi.org/10.1002/jbm.1247.

[47] C.C. Liu, J.K. Yeh, J.F. Aloia, Magnesium directly stimulates osteoblast proliferation, J. Bone Miner. Res. 3 (1988) 104.

[48] C. Wu, J. Chang, W. Zhai, S. Ni, J. Wang, Porous akermanite scaffolds for bone tissue engineering: preparation, characterization, and in vitro studies, J. Biomed. Mater. Res. B Appl. Biomater. 78 (2006) 47–55.

[49] Y. Kang, S. Kim, M. Fahrenholtz, A. Khademhosseini, Y. Yang, Osteogenic and angiogenic potentials of monocultured and co-cultured human-bone-marrow-derived mesenchymal stem cells and human-umbilical-vein endothelial cells on three-dimensional porous beta-tricalcium phosphate scaffold, Acta Biomater. 9 (2013) 4906–4915, https://doi.org/10.1016/j.actbio.2012.08.008.

[50] H.R. Bakhsheshi, M. Akbari, A.F. Ismail, M. Aziz, Z. Hadisi, E. Pagan, M. Daroonparvar, X. Chen, Coating biodegradable magnesium alloys with electrospun poly-L-lactic acid-åkermanite-doxycycline nanofibers for enhanced biocompatibility, antibacterial activity, and corrosion resistance, Surf. Coat. Technol. 377 (2019), 124898.

[51] R. Sánchez-Clemente, M.I. Igeño, A.G. Población, M.I. Guijo, F. Merchán, R. Blasco, Study of pH changes in media during bacterial growth of several environmental strains, Proceedings 2 (2018) 1297, https://doi.org/10.3390/proceedings2201297.

[52] I. Allan, H. Newman, M. Wilson, Antibacterial activity of particulate Bioglass® against supra- and subgingival bacteria, Biomaterials 22 (2001) 1683–1687, https://doi.org/10.1016/S0142-9612(00)00330-6.

[53] Q. Jin, M.F. Kirk, pH as a primary control in environmental microbiology, Front. Environ. Sci. 6 (2018), https://doi.org/10.3389/fenvs.2018.00021.